ACS Sustainable Chemistry & Engineering

pubs.acs.org/journal/ascecg

Research Article

Titanium-Containing Metal–Organic Framework Modified Separator for Advanced Lithium–Sulfur Batteries

Chu Qi, Lin Xu, Jia Wang, Huilan Li, Chengcheng Zhao, Lina Wang,* and Tianxi Liu*

Cite This: *ACS Sustainable Chem. Eng.* 2020, 8, 12968–12975

Read Online

ACCESS | Metrics & More | Article Recommendations | Supporting Information

ABSTRACT: The shuttling of polysulfide intermediates (Li_2S_n, $2 < n \leq 8$) and the dendrite growth on the Li-metal surface have blocked the practical applications of lithium–sulfur (Li–S) batteries. Functionalizing the separator provides a straightforward approach to address these issues. Herein, we demonstrate a multifunctional MIL-125(Ti)-modified polypropylene/polyethylene separator for advanced Li–S batteries. The MIL-125(Ti), a Ti-containing metal–organic framework (MOF), features an open-skeleton construction, a high intrinsic microporosity and a Lewis acid characteristic. Compared with pristine separator, that with MIL-125(Ti) coating shows better electrolyte wettability and less resistance. The unique coating layer acts as an effective physical and chemical barrier region to capture polysulfide species without affecting the smooth transport of Li^+. Meanwhile, the highly ordered micropores with a diameter of ~1.5 nm in the MOFs guide in a homogeneous Li^+ plating and thereby inhibit lithium dendrites. Consequently, the MOF-modified separator enables a significantly improved cycling stability and rate capability of the Li–S battery. The capacity retention of over 60% at 0.2 C (1 C = 1675 mA g^{-1}) upon 200 cycles and a specific capacity of 612 mAh g^{-1} at 2 C is realized. The facile approach offers an effective pathway toward high-performance Li–S batteries.

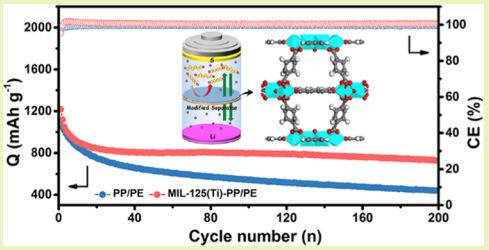

KEYWORDS: *lithium–sulfur battery, metal–organic framework, separator, shuttle effect, lithium dendrites*

INTRODUCTION

With the increasing requirement of electronic devices and electric vehicles, the energy storage systems with high energy density and low cost are in urgent need.[1,2] Further development of the traditional lithium-ion batteries is limited by the low energy density (<300 Wh kg^{-1}) of the transition-metal intercalation compounds. Lithium–sulfur (Li–S) battery is recognized as one of the most promising candidates due to the extremely high theoretical capacity (1675 mAh g^{-1}) and energy density (2600 Wh kg^{-1}) of elemental sulfur (S_8).[3−6] The natural abundance and environmental friendliness of sulfur are additional advantages. Nevertheless, the practical application of Li–S batteries is hindered by tough challenges stemming from the generation of soluble lithium polysulfide intermediates (Li_2S_n, $2 < n \leq 8$) and the use of the very active metallic Li anode.[7,8] The back and forth of Li_2S_n across the widely used microporous separator creates a shuttle effect in the cell. The internal parasitic reactions between Li_2S_n and Li anode induce a low utilization of sulfur and serious corrosion of the Li-anode surface. Besides, the formation of Li dendrites on the Li-anode surface remains an unresolved safety issue.

Majority of on-going efforts are focused on novel cathode matrix, such as physical trapping of Li_2S_n within porous carbons[9] and chemical attaching of Li_2S_n with polar molecules like metal oxides/sulfides/nitrides.[10−17] Beyond that, a separator is another important component and plays a crucial role in determining the cell performance. The separator was designed to prevent electrical shorts by keeping negative and positive electrodes apart while allowing ionic transport between the electrodes. However, the conventional polypropylene (PP)/polyethylene (PE) separators with micropores in tens to hundred nanometers are unable to restrain the diffusion of Li_2S_n. Proper selection of a separator is critical for better battery performance while maintaining the required safety feature. Metal–organic frameworks (MOFs) as a class of porous coordination polymers have been widely used in various fields like gas storage, separation, catalysis, and drug delivery.[18−21] The characteristics of highly uniform (sub-) nanometer-sized pore structures make MOFs promising candidate materials to construct separators. For example, Zhou et al. firstly reported a MOF@graphene oxide separator, which was employed as an ion sieve to restrict the diffusion of polysulfides.[22] Wu et al. constructed a carbon nanotube@ZIF-8 coating layer on one side of PP separator to trap the polysulfides.[23] Hong et al. used cerium-based MOFs combined with carbon nanotube as the separator coating material to catalyze the conversion of polysulfides.[24] He et al. demon-

Received: May 12, 2020
Revised: July 22, 2020
Published: August 4, 2020

https://dx.doi.org/10.1021/acssuschemeng.0c03536
ACS Sustainable Chem. Eng. 2020, 8, 12968–12975

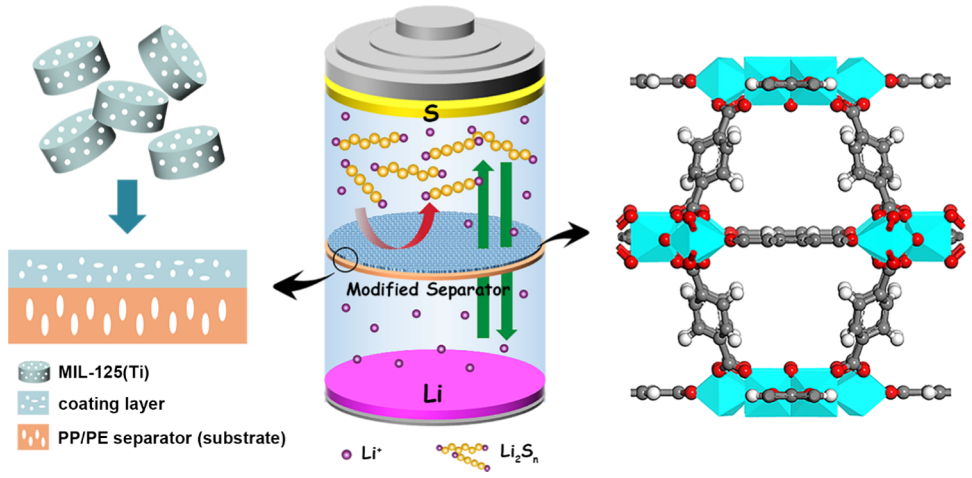

Figure 1. Schematic illustration of the Li−S battery with the MIL-125(Ti)-modified PP/PE separator.

strated a MOF-based bifunctional separator using HKUST-1 nanoparticles to simultaneously suppress the shuttle effect and growth of Li dendrites.[25] While progress in MOF-modified separator significantly improved battery performance, further advancement is still required for practical use. In addition to electrochemical compatibility, several factors such as resource abundance, environmental friendliness, and technology feasible should also be within considerations for the design of separators.

Here, a resourceful Ti-based titanium-*p*-phthalic acid MOF, namely, MIL-125(Ti) ($Ti_8O_8(OH)_4(BDC)_6$, BDC = 1,4-benzene dicarboxylate), was prepared from a solvothermal process and employed as a barrier region of separator for Li−S batteries. The MIL-125(Ti) coating layer on the PP/PE membrane acts as an effective physical and chemical barrier region to capture polysulfide species without affecting the smooth transport of Li^+. The three-dimensional open skeleton of the MOF particles with a large surface area (1386 $m^2\ g^{-1}$) and uniform micropores (~1.5 nm) guarantees the fast transportation of Li^+ and guides in a homogeneous Li plating/stripping.[26,27] Also, the strong binding ability between O atoms from the BDC ligands in MIL-125(Ti) and Li^+ ions in Li_2S_n leads to the immobilization of S_n^{2-}.[28−30] As a result of the synergistic effects, the microporous PP/PE membrane modified by a MIL-125(Ti) coating layer could effectively suppress the polysulfide shuttle and the Li-dendrite growth, evidenced in terms of the high cyclic stability and rate performance. Even when a relatively low current rate of 0.2 C (1 C = 1675 mA g^{-1}) is applied, a low capacity decay of 0.2% per cycle is achieved over 200 cycles.

EXPERIMENTAL SECTION

Preparation of MIL-125(Ti). MIL-125(Ti) was synthesized according to a solvothermal process.[31] In detail, 3 g of 1,4-benzenedicarboxylic acid (H_2BDC, Aladdin, 99%) was added into a 100 mL beaker containing 54 mL of *N*,*N*-dimethylformamide (DMF, Sinopharm Chemical, ≥99.0%) and 6 mL of anhydrous methanol (Sinopharm Chemical, ≥99.7%). The mixture solution was stirred continuously. Then, 1.56 mL of tetra-*n*-butyl titanate $Ti(OC_4H_9)_4$ (Sigma-Aldrich, 97%) was added into the solution quickly. After stirring for 4 h, the resulted mixture was transferred into a Teflon-lined autoclave and heated at 150 °C for 24 h. The MIL-125(Ti) powder was collected after centrifugation and drying at 60 °C under vacuum overnight.

Preparation of MIL-125(Ti)-PP/PE Separator. In preparing the modified separator, a black viscous slurry consisting of 90% as-synthesized MIL-125(Ti) and 10% poly(vinylidene fluoride) (PVdF, HSV900) in *N*-methyl-2-pyrrolidone (NMP, Shanghai Lingfeng Chemical, ≥99.0%) was prepared first. Then, the slurry was cast onto a PP/PE microporous membrane (Celgard 2325, 25 μm thick). Finally, the membrane was dried in a vacuum oven at 50 °C for 12 h to obtain the MIL-125(Ti) modified PP/PE separator. The MIL-125(Ti)-PP/PE separator was punched into circular disks with a diameter of 18 mm for the following cell assembly.

Preparation of Li_2S_6 Solution. The Li_2S_6 (5 mM) solution was prepared by adding sulfur and Li_2S at a molar ratio of 5:1 in the solvent of 1,3-dioxolane/dimethoxyethane (DOL/DME, v/v = 1:1) in an Ar-filled glovebox.

Material Characterizations. The X-ray diffraction (XRD) patterns were measured on an X-ray diffractometer with Cu Kα radiation (D/max-2550VB+/PC, Rigalcu). Scanning electron microscopy (SEM) and energy-dispersive X-ray spectroscopy (EDS) was performed on JSM-7500F and Talos F200S instruments, respectively. The nitrogen sorption/desorption was measured on a Quadrasorb adsorption instrument (ASIQMUOOUOO-6, Quantachrome). The apparent surface area was calculated using the Brunauer−Emmett−Teller (BET) method. The pore size distributions were calculated using the nonlocal density functional theory (NLDFT) equilibrium model method. The mechanical properties of the separators were carried by an electronic universal testing machine (UTM2102, SUNS). The contact angles were measured on an optical contact angle measuring device (OCA 40Micro, Dataphysics) using the electrolyte solution of 1 M bis(trifluoromethane)sulfonimide lithium salt (LiTFSI) in 1,3-dioxolane (DOL)/dimethoxymethane (DME) (v/v = 1:1) in the presence of 0.2 M $LiNO_3$ additive. The porosity was determined by immersing the separator into *n*-butanol for 2 h and calculating based on the following equation: porosity (%) = $[(m_b/\rho_b)/(m_b/\rho_b + m_a/\rho_a)] \times 100\%$, where m_a and m_b is the mass of the separator and *n*-butanol and ρ_a and ρ_b are the densities of separator and *n*-butanol, respectively.

Electrochemical Measurements. All of the materials for the preparation of the cathode were thoroughly dried before use. The CR2025-type coin cells were assembled in an argon-filled glovebox with H_2O and O_2 contents below 0.1 ppm (Mikrouna). In preparation of cathodes for Li−S cells, the homogeneous slurry consisting of 70 wt % elemental sulfur (Sinopharm Chemical), 20 wt % Ketjen Black (ECP-600JD) and 10 wt % PVdF in *N*-methyl-2-pyrrolidone (NMP, ≥99.0%) were cast on an Al foil (18 μm thick). After being dried in a vacuum oven at 60 °C, the electrodes were cut into circular disks with a diameter of 12 mm. The thickness of the electrode is about 40 μm and the sulfur loading is 2 mg cm^{-2}. Metallic lithium was used as the anode. The electrolyte used was 1 M LiTFSI in DOL/DME (v/v =

https://dx.doi.org/10.1021/acssuschemeng.0c03536
ACS Sustainable Chem. Eng. 2020, 8, 12968−12975

1:1) with 0.2 M $LiNO_3$ additive. The electrolyte amount was controlled at ~40 μL in each cell.

Cyclic voltammetry (CV) was tested in the potential range of 1.7−2.7 V (vs Li/Li^+) at various scan rates at an Arbin workstation (Arbin Instruments). Electrochemical impedance spectroscopy (EIS) was measured in the range of 0.01 Hz to 1000 kHz at a potentiostatic signal amplitude of 5 mV on a CHI660E electrochemical workstation (Shanghai Chenhua, China). The galvanostatic charge−discharge was operated within 1.7 and 2.7 V (vs Li/Li^+) on a NEWARE cell test system (Shenzhen, China). For comparison, the cells with pristine PP/PE separator were also assembled and tested as mentioned above.

Computational Methods. The calculation of the binding energies between Ti(IV) octaxanuclear cluster and polysulfide (Li_2S_6) was conducted by density functional theory (DFT) within the framework of the Dmol3 package combined with the Perdew−Berke−Ernzerhof of generalized gradient approximation (GGA-PBE). The double numerical plus polarization (DNP) basis sets with effective core potential was used to denote the atomic potentials. Additionally, the self-consistent field (SCF) tolerance was less than 1×10^{-6}. The adsorption energy between segments of Ti(IV) octaxanuclear cluster and adsorbed polysulfides (for example, Li_2S_6) is determined by $E_a = E_{seg.} + E_{Li_2S_6} - E_{Li_2S_6@seg.}$, where $E_{Li_2S_6}$ is the total energies of the adsorbed polysulfide, $E_{seg.}$ and $E_{Li_2S_6@seg.}$ are the segment of Ti(IV) octaxanuclear cluster and the polysulfide−Ti(IV) octaxanuclear cluster, respectively.

RESULTS AND DISCUSSION

Preparation and Material Characterizations of MIL-125(Ti)-PP/PE Separator. As shown in Figure 1, the Ti-MOF-modified separator was prepared by casting a mixture of MIL-125(Ti) and PVdF binder onto a PP/PE membrane. MIL-125(Ti) coating is designed to serve as a physical and chemical barrier for soluble polysulfides. The intercalations between polysulfides and MIL-125(Ti) were quantitatively illustrated by the adsorption energy calculation, which reflects the immobilizing ability of polysulfides on the MIL-125(Ti) framework. The structure, metal nodes, and the Li_2S_6 adsorption sites in MIL-125(Ti) are shown in Figure 2a. The calculated binding energy (E_b) between Li_2S_6 and MIL-125(Ti) framework (2.27 eV) indicates an outstanding interaction, which arises from the strong binding ability between O atoms from the BDC ligands in MIL-125(Ti) and Li^+ ions in Li_2S_6. Similar high E_b values are obtained between other intermediate polysulfides with MIL-125(Ti) as well (Figure S1). Such chemical adsorption would result in a mitigated shuttle effect in Li−S batteries. The adsorption experiment was conducted to further evaluate the interaction between the MIL-125(Ti) and Li_2S_n. As illustrated in Figure S2, the MIL-125(Ti) was added into the 5 mM Li_2S_6 solution. Along with the increase in time, the color of the solution containing MIL-125(Ti) appears more and more light compared with the reference Li_2S_6 solution, indicating the interaction between the MIL-125(Ti) and Li_2S_n. XPS of MIL-125(Ti) after adsorbing Li_2S_6 provides more convincing evidence. As shown in Figure 2b, the O 1s spectrum of pristine MIL-125(Ti) is composed of three contributions at 532.18, 531.67, and 530.25 eV, which is assigned to the O−H, C═O, and Ti−O bonds, respectively. In contrast, for the MIL-125(Ti) after adsorbing Li_2S_6, an additional peak ascribed to the Li−O bond emerged at 530.97 eV. Furthermore, we also investigated the Ti 2p spectrum of the MIL-125(Ti) before and after the adsorption experiment (Figure S3). Before adsorption, two sharp peaks appearing at 458.89 and 464.65 eV are related to Ti $2p_{3/2}$ and Ti $2p_{1/2}$, respectively. Obviously, the peaks of Ti $2p_{1/2}$ and Ti $2p_{3/2}$ are barely shifted after adsorption, manifesting no change in the valence state of Ti. According to the above analysis, it is confirmed that the chemisorption between the MIL-125(Ti) and polysulfides is generated from the interactions between O atoms in MIL-125(Ti) and Li atoms in polysulfides.

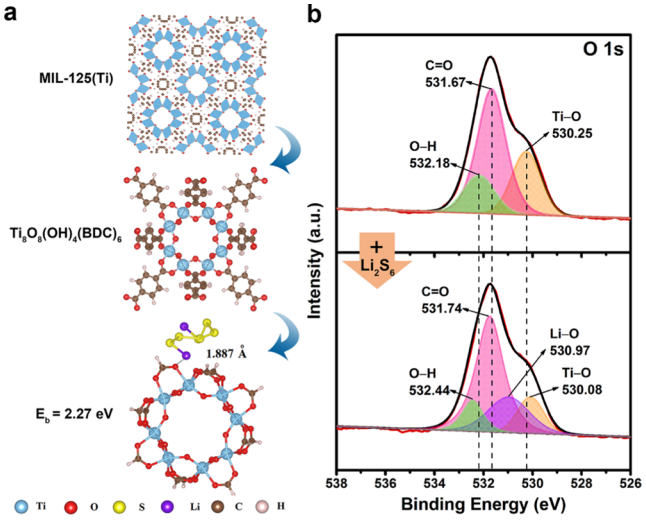

Figure 2. (a) Optimized stable structure of adsorption configuration between Li_2S_6 and MIL-125(Ti). (b) High-resolution O 1s XPS spectrum of MIL-125(Ti) before and after adsorption of Li_2S_6.

The MIL-125(Ti) was synthesized via a simple solvothermal method. Scanning electron microscopy (SEM) shows that the particles of the as-prepared sample appear as uniform disks with a smooth surface (Figure 3a). The size of the particles is in the range of 1.5−2 μm in diameter (Figure 3b). Energy-dispersive X-ray spectroscopy (EDS) analysis shows the homogeneous distribution of O, C, and Ti elements throughout the particles (Figure 3c). The crystalline structure of the as-synthesized sample is confirmed by the X-ray diffractometer (XRD) analysis (Figure 3d). The visible main diffraction peaks at 2θ = 6.8, 9.8 11.7, 15.1, 15.5, 16.6, 17.9, 19.1, 19.6, and 22.7° can be well indexed to a space group of $I4/mmm$ (n°139), corresponding to the MIL-125(Ti) crystals.[32,33] Porous characteristic is identified by N_2 adsorption measurement. The evacuated MIL-125(Ti) exhibits type I isotherms with a rapid increase in N_2 uptake at a low relative pressure (<0.01), suggesting the microporous structure (Figure 3e).[34] The Brunauer−Emmett−Teller (BET) surface area is calculated to be 1386.13 $m^2\ g^{-1}$, allowing full contact with the electrolyte. The pore diameter is concentrated at 1.5 nm (Figure 3f), which would restrict larger molecules, such as long-chain polysulfides, from diffusing across the pores freely.

The widely used microporous PP/PE membrane generally exhibits uniformly interconnected elliptic pores ranging from tens to hundreds of nanometers (Figure 4a,b). The large pores are unable to restrain the free shuttle back and forth of polysulfides, causing the severe shuttle effect in a Li−S cell.[35−37] Apparently, the game shift to a functionalized separator is essential for an improved Li−S battery. The slurry of MIL-125(Ti) crystals with PVdF binder was cast on the single side of the PP/PE separator. The top-view SEM images indicate a homogeneous dispersion of MIL-125(Ti) (Figure 4c) and the discal particles are well preserved (Figure 4d). The cross-sectional view of SEM in Figure 4e shows that the dense coating layer holds a thickness of 20 μm. The coating layer

https://dx.doi.org/10.1021/acssuschemeng.0c03536
ACS Sustainable Chem. Eng. 2020, 8, 12968−12975

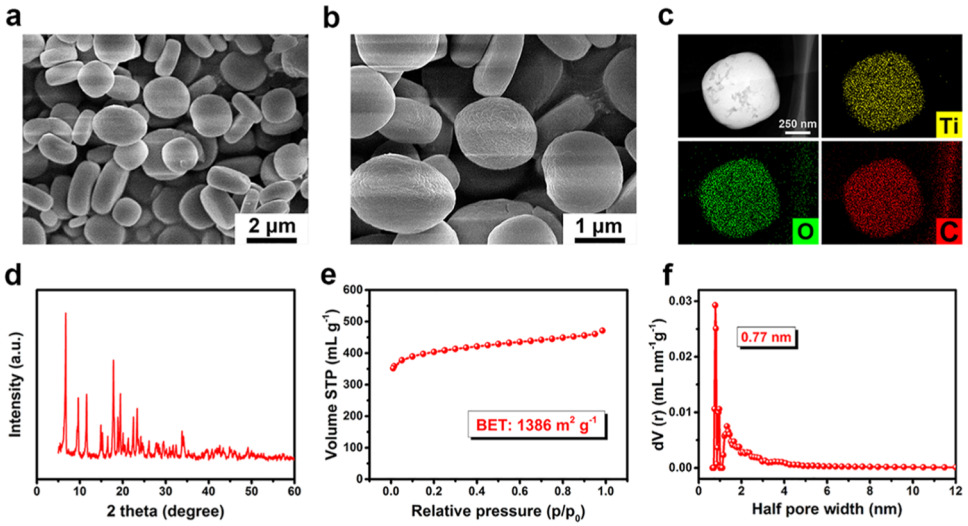

Figure 3. Characterization of the as-synthesized MIL-125(Ti). (a, b) SEM images. (c) Elemental mapping images of Ti, O, and C. (d) XRD. (e) Nitrogen adsorption−desorption curve. (f) Pore size distribution.

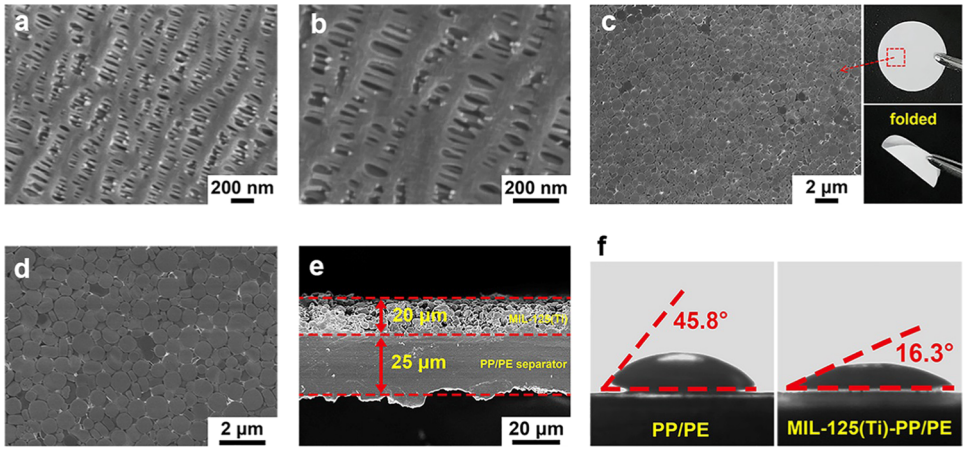

Figure 4. (a, b) SEM images of pristine PP/PE separator. (c, d) Top-view and (e) sectional SEM images of MIL-125(Ti)-PP/PE separator. (f) Contact angle of PP/PE and MIL-125(Ti)-PP/PE separator.

keeps a good mechanical property that would not affect the flexibility of the separator. The stress−strain behavior along the machine direction (M) and the transversal direction (T) is shown in Figure S4. The elongation at break of the MIL-125(Ti)-PP/PE separator (89%) is improved without the loss of tensile strength along the machine direction. The structural integrity of the MIL-125(Ti) layer generally can be maintained after stretching, as shown in the SEM images in Figure S5. The surface wettability of the electrolyte plays a crucial factor for the separator with good Li-ion conductivity. The contact angle of the pristine PP/PE membrane is 45.8°, which is reduced to 16.3° after the decoration of MIL-125(Ti) (Figure 4f). Indeed, the porosity of the modified separator (53.32%) is fairly higher than that of the PP/PE membrane (42.17%) as shown in Table S1. The improved affinity to electrolyte would result in a high ionic conductivity of the electrolyte-soaked separator.

The feasibility of the MIL-125(Ti)-PP/PE separator for a physical restriction of polysulfides is probed via a visible permeation test. As illustrated in Figure 5a, a glass vial loaded with a yellowish polysulfide solution (5 mM Li_2S_6) with an open hole was sealed with a piece of a separator. The upturned vial was immersed into a blank electrolyte. From the observation of the color change in the outside blank solution, as shown in Figure 5b, it can be seen that the polysulfides could easily cross the bare PP/PE separator. However, the polysulfides could hardly permeate the MIL-125(Ti)-PP/PE separator within 12 h (Figure 5c), showing the promising prospect to be used in Li−S batteries.

Electrochemical Characteristics of MIL-125(Ti)-PP/PE Separator. To verify the effectiveness of the MIL-125(Ti)-PP/PE separator in Li−S batteries, electrochemical characteristics were investigated with CR2025-type coin cells. Figure 6a shows the cyclic voltammetry (CV) curves of Li−S cells with MIL-125(Ti)-PP/PE and bare PP/PE separators, respectively. Both of the cells exhibit a pair of cathodic peaks at 1.8−2.0 and 2.1−2.3 V, corresponding to the ring-opening reduction reaction of cyclo-S_8 to long-chain soluble Li_2S_n ($4 \leq n \leq 8$) and further to solid Li_2S_2/Li_2S, respectively. Also, the anodic peak at 2.4−2.5 V is associated with the oxidation of Li_2S_2/Li_2S back to S_8. The voltage polarization between the cathodic and anodic peaks of the cell with MIL-125(Ti)-PP/PE is reduced compared with that with the PP/PE separator, indicating an improved reaction dynamics. The results are compatible with the voltage hysteresis (ΔE) in the charge−discharge profiles (Figure 6b). The ΔE of the cell with MIL-125(Ti)-PP/PE separator is 0.18 eV, smaller than that of 0.25 eV with the PP/

https://dx.doi.org/10.1021/acssuschemeng.0c03536
ACS Sustainable Chem. Eng. 2020, 8, 12968−12975

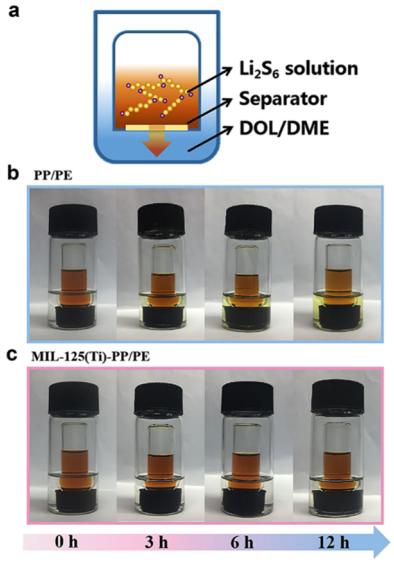

Figure 5. (a) Diagram of polysulfide solution across the separator. Time-dependent diffusion of Li_2S_6 solution in the visualized bottle with (b) PP/PE and (c) MIL-125(Ti)-PP/PE separator.

PE separator. The electrochemical difference between the two cells suggests that the MIL-125(Ti) coating layer positively affects the battery performance.

The rate performance was evaluated at various current rates. As shown in Figure 6c, the average specific capacities of MIL-125(Ti)-PP/PE and PP/PE separator are 1011/925, 822/698, 748/608, 687/560, and 592/495 mAh g^{-1} at 0.1 (1 C = 1675 mA g^{-1}), 0.2, 0.5, 1, and 2 C, respectively. The corresponding voltage profiles of the two types of cells are shown in Figure S6. Clearly, the MIL-125(Ti)-PP/PE separator delivers higher specific capacity, a smaller voltage hysteresis at each current rate, indicating a higher efficiency of sulfur utilization. The cycle stability of the Li−S cells over 200 cycles is shown in Figure 6d. Upon 0.2 C, the cell with MIL-125(Ti)-PP/PE separator shows a higher initial discharge capacity of 1218.3 mAh g^{-1}, while that with PP/PE separator delivers a specific capacity of 1108.4 mAh g^{-1}. Up to 200 cycles, a highly reversible capacity of 726 mAh g^{-1} remains for the cell with the MIL-125(Ti)-PP/PE separator. The lower discharge plateau was mainly stable at a similar voltage during the whole cycling process without a distinct voltage drop, indicating the reaction kinetics are always kept at a rapid level (Figure S7). However, merely 439 mAh g^{-1} is retained for the cell with the PP/PE separator. The performance of MIL-125(Ti)-PP/PE is among the top results in comparison to previously reported MOF-modified separators (Table S2), showing the great promise in high-performance Li−S batteries. The cycled cells were detached to observe the state of Li electrodes, and the bare Li foil is given as a contrast (Figure S8). A damaged surface in dark color is observed from the Li foil with PP/PE separator (inset in Figure 6e), while the Li anode with MIL-125(Ti)-PP/PE separator shows a much clean surface (inset in Figure 6f). The SEM images of the Li-anode surface provide more convincing evidence. The Li anode with the PP/PE separator shows an uneven surface with rough deposits and massive cracks (Figure 6e), resulting from severe polysulfide-induced corrosion as well as dendritic Li growth. A smooth surface is observed on the Li-anode surface with the MIL-125(Ti)-PP/PE separator (Figure 6f), suggesting that the polysulfide shuttling is well regulated and the growth of Li dendrites are suppressed by the MIL-125(Ti) barrier. The result is consistent with the previous reports, which have suggested that the liquid electrolyte-filled specific MOF membranes could aid in guiding the uniformity of Li-ion plating.[38]

The above analysis suggests that the modified separator is effective in mitigating the shuttle of the polysulfides. Through the adsorption effects, soluble Li_2S_n were efficiently immobilized at the cathode side, which reduced their shuttle to the anode. Also, on the other hand, the as-adsorbed polysulfides may accumulate on the separator toward the cathode side and hamper redox kinetics.[39] However, compared with the uncontrolled loss of active sulfur from the shuttle of Li_2S_n, the side effect from the adsorbed polysulfides on separator should be limited. The electrochemical impedance spectroscopy (EIS) was measured to verify whether MIL-125(Ti) can promote Li^+ transfer across the separator. Also, the simulation equivalent circuit is also provided. As shown in Figure 7a, the Nyquist plots of both the cells are comprised of a semicircle at

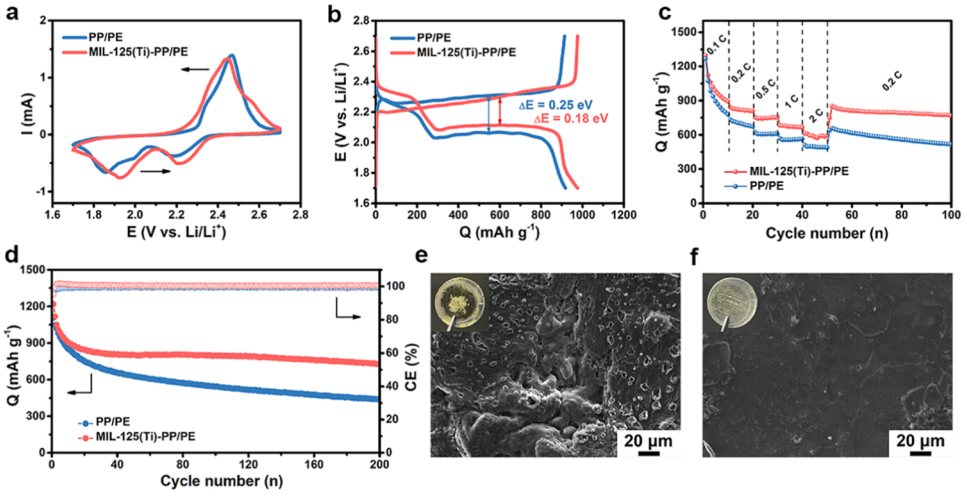

Figure 6. Electrochemical characteristics of Li−S batteries with PP/PE or MIL-125(Ti)-PP/PE separator. (a) CV curves at 0.1 mV s^{-1}. (b) Galvanostatic charge−discharge profiles at 0.2 C. (c) Rate capability. (d) Cyclic performance at 0.2 C. The surface morphologies along with the optical images (insets) of cycled Li anodes with (e) PP/PE and (f) MIL-125(Ti)-PP/PE separator.

https://dx.doi.org/10.1021/acssuschemeng.0c03536
ACS Sustainable Chem. Eng. 2020, 8, 12968−12975

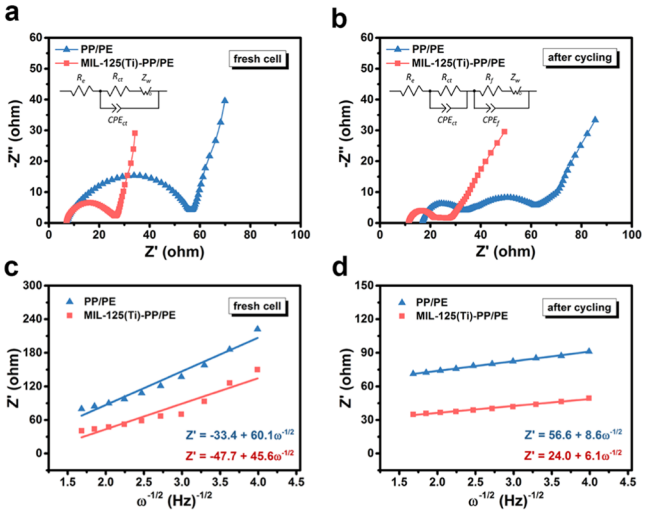

Figure 7. EIS profiles and the corresponding equivalent circuit (insets) of the Li−S cells with a PP/PE or MIL-125(Ti)-PP/PE separator (a) before and (b) after 100 cycles. Correlation between Z' and $\omega^{-1/2}$ at low frequency derived from EIS results (c) before and (d) after 100 cycles.

the high frequency and a sloping line at the low frequency, which can be assigned to the charge-transfer resistance (R_{ct}) and Warburg impedance (Z_W), respectively. The x-intercept represents the Ohmic resistance of electrolyte (R_e). Obviously, the EIS spectrum of MIL-125(Ti)-PP/PE separator manifests the faster reaction kinetics by showing a considerably smaller resistance compared to bare PP/PE membrane. A new semicircle ascribed to the formation of solid electrolyte interphase (SEI) at the anode surface appears at the medium frequency for the cycled cells (Figure 7b), which is manifested by R_f in the simulation equivalent circuit.[40] The rapid Li^+ transfer is related to the full contact with electrolyte supported by the high specific surface area of MIL-125(Ti). To further demonstrate the ion transfer properties, the corresponding linear fits between the real part Z' impedance versus the $\omega^{-1/2}$ at low frequency are given in Figure 7c,d, where ω is the angular frequency. The Li^+ diffusion coefficient (D_{Li}) is determined by the slope σ_W (Warburg coefficient) of fitting lines.[41] It can be seen that the MIL-125(Ti)-PP/PE separator consistently exhibits the smaller slope before and after cycling, indicating the faster Li^+ transfer during the charge−discharge process. The ionic conductivity in the electrolyte-filled pore space of separators is not only a function of the electrolyte properties but also the structure of the separator. The result manifests that the MIL-125(Ti) can promote Li^+ transfer across the separator. Also, it is reasonable to speculate that the fast Li^+ transfer could reactivate the absorbed polysulfides on a separator to continue the redox reaction at the cathode side.

The Li^+ plating behavior affected by the MIL-125(Ti)-PP/PE and PP/PE separator was also employed in Li||Cu cells. Figure S9a shows the Coulombic efficiency (CE) of the Li||Cu cells with different separators at a current density of 1 mA cm^{-2}. It can be seen that the CE of the cell with PP/PE separator sharply declines after the 25th cycle. In contrast, a CE of 91.5% is remained for the cell with MIL-125(Ti)-PP/PE separator after 100 cycles. Also, the corresponding charge/discharge profiles are nearly overlapped with a smaller voltage hysteresis of ∼45 mV (Figure S9b). The result suggests that the 3D open skeleton and uniform microporous size of MIL-125(Ti) can guide the uniform Li^+ plating, which is further convinced by the Li||Li symmetric cells tested at 1 mA cm^{-2} with a capacity of 1 mAh cm^{-2} (Figure S9c). The even Li^+ plating/stripping of the cell with MIL-125(Ti)-PP/PE separator leads to a stable overpotential of ∼40 mV over 300 h. However, the fluctuant and huge overpotential of the cell with PP/PE separator reflects the uncontrollable Li^+ plating/stripping behavior.

CONCLUSIONS

In summary, a multifunctional separator was fabricated by introducing a homogeneous MIL-125(Ti) coating layer on a conventional PP/PE separator. The microporous structure of MIL-125(Ti) with an extremely small pore size of ∼1.5 nm not only allows the fast transportation of Li^+ as well as regulates the Li plating/stripping behavior. The Lewis base−acid interaction between MIL-125(Ti) and Li_2S_n also plays a critical role in mitigating the shuttle effect. Therefore, the Li−S batteries with the MIL-125(Ti)-PP/PE separator exhibit high cycling stability and improved rate capability. This work demonstrates a facile and valid approach for achieving high-performance Li−S batteries.

ASSOCIATED CONTENT

Supporting Information

The Supporting Information is available free of charge at https://pubs.acs.org/doi/10.1021/acssuschemeng.0c03536.

Porosity measurement, calculated adsorption energy between polysulfides and MIL-125(Ti), polysulfide adsorption experiment, Ti 2p XPS spectrum of MIL-125(Ti), mechanical properties of separators, characterization of the separator after stretching, rate capability of Li−S cells, cyclic performance of Li−S cells at 0.2 C, comparison of different MOF-modified separators for Li−S batteries, morphology of bare Li anode, and performance of Li||Cu and Li||Li symmetric cells (PDF)

AUTHOR INFORMATION

Corresponding Authors

Lina Wang − *State Key Laboratory for Modification of Chemical Fibers and Polymer Materials, College of Materials Science and Engineering, Innovation Center for Textile Science and Technology, Donghua University, Shanghai 201620, China;* orcid.org/0000-0002-2211-4661; Email: linawang@dhu.edu.cn

Tianxi Liu − *State Key Laboratory for Modification of Chemical Fibers and Polymer Materials, College of Materials Science and Engineering, Innovation Center for Textile Science and Technology, Donghua University, Shanghai 201620, China; Key Laboratory of Synthetic and Biological Colloids, Ministry of Education, School of Chemical and Material Engineering, Jiangnan University, Wuxi 214122, China;* Email: txliu@dhu.edu.cn

Authors

Chu Qi − *State Key Laboratory for Modification of Chemical Fibers and Polymer Materials, College of Materials Science and Engineering, Innovation Center for Textile Science and Technology, Donghua University, Shanghai 201620, China*

Lin Xu − *State Key Laboratory for Modification of Chemical Fibers and Polymer Materials, College of Materials Science and*

https://dx.doi.org/10.1021/acssuschemeng.0c03536
ACS Sustainable Chem. Eng. 2020, 8, 12968−12975

Engineering, Innovation Center for Textile Science and Technology, Donghua University, Shanghai 201620, China

Jia Wang − *State Key Laboratory for Modification of Chemical Fibers and Polymer Materials, College of Materials Science and Engineering, Innovation Center for Textile Science and Technology, Donghua University, Shanghai 201620, China*

Huilan Li − *State Key Laboratory for Modification of Chemical Fibers and Polymer Materials, College of Materials Science and Engineering, Innovation Center for Textile Science and Technology, Donghua University, Shanghai 201620, China*

Chengcheng Zhao − *State Key Laboratory for Modification of Chemical Fibers and Polymer Materials, College of Materials Science and Engineering, Innovation Center for Textile Science and Technology, Donghua University, Shanghai 201620, China*

Complete contact information is available at: https://pubs.acs.org/10.1021/acssuschemeng.0c03536

Author Contributions

The manuscript was written through contributions of all authors. All authors have given approval to the final version of the manuscript.

Notes

The authors declare no competing financial interest.

■ ACKNOWLEDGMENTS

The authors gratefully acknowledge funding support from the Fundamental Research Funds for the Central Universities (2232018D3-02 and 2232019D3-10) and the Shanghai Scientific and Technological Innovation Project (18JC1410600).

■ REFERENCES

(1) Whittingham, M. S. Lithium Batteries and Cathode Materials. *Chem. Rev.* **2004**, *104*, 4271−4302.

(2) Bruce, P. G.; Freunberger, S. A.; Hardwick, L. J.; Tarascon, J.-M. Li−O_2 and Li−S Batteries with High Energy Storage. *Nat. Mater.* **2012**, *11*, 19−29.

(3) Wang, L.; Liu, J.; Yuan, S.; Wang, Y.; Xia, Y. To Mitigate Self-Discharge of Lithium−Sulfur Batteries by Optimizing Ionic Liquid Electrolytes. *Energy Environ. Sci.* **2016**, *9*, 224−231.

(4) Yin, Y.-X.; Xin, S.; Guo, Y.-G.; Wan, L.-J. Lithium−Sulfur Batteries: Electrochemistry, Materials, and Prospects. *Angew. Chem., Int. Ed.* **2013**, *52*, 13186−13200.

(5) Wang, X.; Qian, Y.; Wang, L.; Yang, H.; Li, H.; Zhao, Y.; Liu, T. Sulfurized Polyacrylonitrile Cathodes with High Compatibility in Both Ether and Carbonate Electrolytes for Ultrastable Lithium−Sulfur Batteries. *Adv. Funct. Mater.* **2019**, *29*, No. 1902929.

(6) Qu, H.; Zhang, J.; Du, A.; Chen, B.; Chai, J.; Xue, N.; Wang, L.; Qiao, L.; Wang, C.; Zang, X.; Yang, J.; Wang, X.; Cui, G. Multifunctional Sandwich-Structured Electrolyte for High-Performance Lithium−Sulfur Batteries. *Adv. Sci.* **2018**, *5*, No. 1700503.

(7) Tang, B.; Wu, H.; Du, X.; Cheng, X.; Liu, X.; Yu, Z.; Yang, J.; Zhang, M.; Zhang, J.; Cui, G. Highly Safe Electrolyte Enabled via Controllable Polysulfide Release and Efficient Conversion for Advanced Lithium−Sulfur Batteries. *Small* **2020**, *16*, No. 1905737.

(8) Zhang, S.; Ueno, K.; Dokko, K.; Watanabe, M. Recent Advances in Electrolytes for Lithium−Sulfur Batteries. *Adv. Energy Mater.* **2015**, *5*, No. 1500117.

(9) Zhang, J.; Yang, C.-P.; Yin, Y.-X.; Wan, L.-J.; Guo, Y.-G. Sulfur Encapsulated in Graphitic Carbon Nanocages for High-Rate and Long-Cycle Lithium−Sulfur Batteries. *Adv. Mater.* **2016**, *28*, 9539−9544.

(10) Wang, J.; Fu, C.; Wang, X.; Yao, Y.; Sun, M.; Wang, L.; Liu, T. Three-Dimensional Hierarchical Porous TiO_2/Graphene Aerogels as Promising Anchoring Materials for Lithium−Sulfur Batteries. *Electrochim. Acta* **2018**, *292*, 568−574.

(11) Li, Z.; Zhang, J.; Lou, X. W. Hollow Carbon Nanofibers Filled with MnO_2 Nanosheets as Efficient Sulfur Hosts for Lithium−Sulfur Batteries. *Angew. Chem., Int. Ed.* **2015**, *54*, 12886−12890.

(12) Zhu, X.; Zhao, W.; Song, Y.; Li, Q.; Ding, F.; Sun, J.; Zhang, L.; Liu, Z. In Situ Assembly of 2D Conductive Vanadium Disulfide with Graphene as a High-Sulfur-Loading Host for Lithium−Sulfur Batteries. *Adv. Energy Mater.* **2018**, *8*, No. 1800201.

(13) Ma, L.; Wei, S.; Zhuang, H. L.; Hendrickson, K. E.; Hennig, R. G.; Archer, L. A. Hybrid Cathode Architectures for Lithium Batteries Based on TiS_2 and Sulfur. *J. Mater. Chem. A* **2015**, *3*, 19857−19866.

(14) Xing, Z.; Li, G.; Sy, S.; Chen, Z. Recessed Deposition of TiN into N-Doped Carbon as a Cathode Host for Superior Li−S Batteries Performance. *Nano Energy* **2018**, *54*, 1−9.

(15) Ma, L.; Yuan, H.; Zhang, W.; Zhu, G.; Wang, Y.; Hu, Y.; Zhao, P.; Chen, R.; Chen, T.; Liu, J.; Hu, Z.; Jin, Z. Porous-Shell Vanadium Nitride Nanobubbles with Ultrahigh Areal Sulfur Loading for High-Capacity and Long-Life Lithium−Sulfur Batteries. *Nano Lett.* **2017**, *17*, 7839−7846.

(16) Li, H.; Wang, X.; Qi, C.; Zhao, C.; Fu, C.; Wang, L.; Liu, T. Self-Assembly of MoO_3-Decorated Carbon Nanofiber Interlayers for High-Performance Lithium−Sulfur Batteries. *Phys. Chem. Chem. Phys.* **2020**, *22*, 2157−2163.

(17) An, Y.; Zhang, Z.; Fei, H.; Xiong, S.; Ji, B.; Feng, J. Ultrafine TiO_2 Confined in Porous-Nitrogen-Doped Carbon from Metal−Organic Frameworks for High-Performance Lithium Sulfur Batteries. *ACS Appl. Mater. Interfaces* **2017**, *9*, 12400−12407.

(18) Li, G.; Kobayashi, H.; Taylor, J. M.; Ikeda, R.; Kubota, Y.; Kato, K.; Takata, M.; Yamamoto, T.; Toh, S.; Matsumura, S.; Kitagawa, H. Hydrogen Storage in Pd Nanocrystals Covered with a Metal-Organic Framework. *Nat. Mater.* **2014**, *13*, 802−806.

(19) Xie, Z.; Li, T.; Rosi, N. L.; Carreon, M. A. Alumina-Supported Cobalt−Adeninate MOF Membranes for CO_2/CH_4 Separation. *J. Mater. Chem. A* **2014**, *2*, 1239−1241.

(20) Jiao, L.; Wang, Y.; Jiang, H.-L.; Xu, Q. Metal-Organic Frameworks as Platforms for Catalytic Applications. *Adv. Mater.* **2018**, *30*, No. 1703663.

(21) Suresh, K.; Matzger, A. J. Enhanced Drug Delivery by Dissolution of Amorphous Drug Encapsulated in a Water Unstable Metal-Organic Framework (MOF). *Angew. Chem., Int. Ed.* **2019**, *58*, 16790−16794.

(22) Bai, S.; Liu, X.; Zhu, K.; Wu, S.; Zhou, H. Metal−Organic Framework-Based Separator for Lithium−Sulfur Batteries. *Nat. Energy* **2016**, *1*, No. 16094.

(23) Wu, F.; Zhao, S.; Chen, L.; Lu, Y.; Su, Y.; Jia, Y.; Bao, L.; Wang, J.; Chen, S.; Chen, R. Metal-Organic Frameworks Composites Threaded on the CNT Knitted Separator for Suppressing the Shuttle Effect of Lithium Sulfur Batteries. *Energy Storage Mater.* **2018**, *14*, 383−391.

(24) Hong, X.-J.; Song, C.-L.; Yang, Y.; Tan, H.-C.; Li, G.-H.; Cai, Y.-P.; Wang, H. Cerium Based Metal-Organic Frameworks as an Efficient Separator Coating Catalyzing the Conversion of Polysulfides for High Performance Lithium−Sulfur Batteries. *ACS Nano* **2019**, *13*, 1923−1931.

(25) He, Y.; Chang, Z.; Wu, S.; Qiao, Y.; Bai, S.; Jiang, K.; He, P.; Zhou, H. Simultaneously Inhibiting Lithium Dendrites Growth and Polysulfides Shuttle by a Flexible MOF-Based Membrane in Li−S Batteries. *Adv. Energy Mater.* **2018**, *8*, No. 1802130.

(26) Rana, M.; Li, M.; Huang, X.; Luo, B.; Gentle, I.; Knibbe, R. Recent Advances in Separators to Mitigate Technical Challenges Associated with Re-Chargeable Lithium Sulfur Batteries. *J. Mater. Chem. A* **2019**, *7*, 6596−6615.

(27) Han, D.-D.; Wang, Z.-Y.; Pan, G.-L.; Gao, X.-P. Metal−Organic-Framework-Based Gel Polymer Electrolyte with Immobilized Anions to Stabilize a Lithium Anode for a Quasi-Solid-State Lithium−Sulfur Battery. *ACS Appl. Mater. Interfaces* **2019**, *11*, 18427−18435.

(28) Pang, Q.; Liang, X.; Kwok, C. Y.; Nazar, L. F. Review—The Importance of Chemical Interactions between Sulfur Host Materials

and Lithium Polysulfides for Advanced Lithium-Sulfur Batteries. *J. Electrochem. Soc.* **2015**, *162*, A2567−A2576.
(29) Zheng, J.; Tian, J.; Wu, D.; Gu, M.; Xu, W.; Wang, C.; Gao, F.; Engelhard, M. H.; Zhang, J.-G.; Liu, J.; Xiao, J. Lewis Acid−Base Interactions between Polysulfides and Metal Organic Framework in Lithium Sulfur Batteries. *Nano Lett.* **2014**, *14*, 2345−2352.
(30) Liang, X.; Garsuch, A.; Nazar, L. F. Sulfur Cathodes Based on Conductive MXene Nanosheets for High-Performance Lithium−Sulfur Batteries. *Angew. Chem., Int. Ed.* **2015**, *54*, 3907−3911.
(31) Fu, Y.; Sun, D.; Chen, Y.; Huang, R.; Ding, Z.; Fu, X.; Li, Z. An Amine-Functionalized Titanium Metal−Organic Framework Photocatalyst with Visible-Light-Induced Activity for CO_2 Reduction. *Angew. Chem., Int. Ed.* **2012**, *51*, 3364−3367.
(32) Dan-Hardi, M.; Serre, C.; Frot, T.; Rozes, L.; Maurin, G.; Sanchez, C.; Férey, G. A New Photoactive Crystalline Highly Porous Titanium(IV) Dicarboxylate. *J. Am. Chem. Soc.* **2009**, *131*, 10857−10859.
(33) Liao, X.; Wei, W.; Zhou, Y.; Zhang, M.; Cai, Y.; Liu, H.; Yao, Y.; Lu, S.; Hao, Q. A Ti-Based Bi-MOF for the Tandem Reaction of H_2O_2 Generation and Catalytic Oxidative Desulfurization. *Catal. Sci. Technol.* **2020**, *10*, 1015−1022.
(34) Msayib, K. J.; Book, D.; Budd, P. M.; Chaukura, N.; Harris, K. D.; Helliwell, M.; Tedds, S.; Walton, A.; Warren, J. E.; Xu, M.; McKeown, N. B. Nitrogen and Hydrogen Adsorption by an Organic Microporous Crystal. *Angew. Chem., Int. Ed.* **2009**, *48*, 3273−3277.
(35) Zhuang, T.-Z.; Huang, J.-Q.; Peng, H.-J.; He, L.-Y.; Cheng, X.-B.; Chen, C.-M.; Zhang, Q. Rational Integration of Polypropylene/Graphene Oxide/Nafion as Ternary-Layered Separator to Retard the Shuttle of Polysulfides for Lithium−Sulfur Batteries. *Small* **2016**, *12*, 381−389.
(36) Huang, J.-Q.; Zhang, Q.; Peng, H.-J.; Liu, X.-Y.; Qian, W.-Z.; Wei, F. Ionic Shield for Polysulfides towards Highly-Stable Lithium−Sulfur Batteries. *Energy Environ. Sci.* **2014**, *7*, 347−353.
(37) Sun, M.; Wang, X.; Wang, J.; Yang, H.; Wang, L.; Liu, T. Assessment on the Self-Discharge Behavior of Lithium−Sulfur Batteries with $LiNO_3$-Possessing Electrolytes. *ACS Appl. Mater. Interfaces* **2018**, *10*, 35175−35183.
(38) Lee, H.; Yanilmaz, M.; Toprakci, O.; Fu, K.; Zhang, X. A Review of Recent Developments in Membrane Separators for Rechargeable Lithium-Ion Batteries. *Energy Environ. Sci.* **2014**, *7*, 3857−3886.
(39) Li, S.; Zhang, W.; Zheng, J.; Lv, M.; Song, H.; Du, L. Inhibition of Polysulfide Shuttles in Li−S Batteries: Modified Separators and Solid-State Electrolytes. *Adv. Energy Mater.* **2020**, No. 2000779.
(40) Wang, Z.; Feng, M.; Sun, H.; Li, G.; Fu, Q.; Li, H.; Liu, J.; Sun, L.; Mauger, A.; Julien, C. M.; Xie, H.; Chen, Z. Constructing Metal-Free and Cost-Effective Multifunctional Separator for High-Performance Lithium-Sulfur Batteries. *Nano Energy* **2019**, *59*, 390−398.
(41) Qin, X.; Wang, X.; Xie, J.; Wen, L. Hierarchically Porous and Conductive $LiFePO_4$ Bulk Electrode: Binder-Free and Ultrahigh Volumetric Capacity Li-Ion Cathode. *J. Mater. Chem.* **2011**, *21*, 12444−12448.

https://dx.doi.org/10.1021/acssuschemeng.0c03536
ACS Sustainable Chem. Eng. 2020, 8, 12968−12975